Kinetic Study of the Devitrification of Mold Powder Slags

Within the continuous casting machine, the mold is the most crucial component. The rate and uniformity of the heat extracted from the strand in the mold, especially near the meniscus, is ultimately responsible for the surface quality of the product and the productivity of the machine. An excessive and/or uneven rate of heat extraction from the newly solidified shell will result in thermally induced stresses that may ultimately cause longitudinal cracks.[1] On the other hand, insufficient mold heat removal may lead to a relatively weak shell that may bulge or tear upon exiting the mold.[2] The phenomena occurring in the interspace between the mold and the solidifying shell, i.e., the formation of the air gap and of the solid and liquid slag layers, control heat transfer and lubrication in the process and therefore are the key to the prevention of cracks and other defects.[3]

The crystallization tendency of the solid slag layer has a large influence on mold heat transfer. A large tendency to form crystalline phases has been reported to be beneficial in the casting of peritectic grades, since a large crystalline fraction reduces the mold heat flux, thereby alleviating longitudinal cracks.[4] The opposite tendency to resist devitrification and remain glassy is required for high-speed casting of low-carbon steels to decrease the possibility of sticking-type breakouts.[4] The influence of crystalline phases on heat transfer is attributed to: formation of pores in the solid layer as a result of the contraction experienced during its formation from the glass phase,[5] widening of the air gap as another result of that contraction[6,7] and scattering of radiation by the crystals, which reduces the radiative portion of the heat flux.[8] Thus, the study of the formation of crystalline phases in the slag layer in the mold-strand gap deserves great attention.

Feldbauer, et al.[9] determined that crystallization of mold slags occurs according to a Time-Temperature-Transformation (TTT) diagram, which is a plot of the isothermal temperature as a function of time needed to crystallize the melt at that temperature. The diagram has a nose shape where the tip corresponds to the temperature, T_n, where the melt, when held isothermally, crystallizes in the shortest possible time (t_n, nose time). A schematic TTT diagram is shown in Figure 1. The slope of the straight line from the liquidus temperature, T_l, to the tip of the nose suggests the critical cooling rate for glass formation, $|\phi_c|(=(T_l - T_n)/t_n)$. This cooling rate is a measure of the ability of a melt to form glass and indicates the slowest rate at which the melt can be cooled from its liquidus temperature without detectable crystallization. The

Due to the rapid cooling of the slag infiltrated into the mold-strand gap, it is expected that the rate of devitrification of the glass formed plays a key role in determining the proportion of crystalline phases influencing mold heat transfer. In this investigation, a novel procedure to calculate Time-Temperature-Transformation curves of mold slags is presented.

Authors

Yadira G. Maldonado
senior engineer for materials development, Material Engineering Area, Chrysler de Mexico S.A de C.V., Cuajimalpa, México
ym93@chrysler.com

F. Andrés Acosta
associate professor, Centre for Research and Advanced Studies, CINVESTAV – Unidad Saltillo, Ramos Arizpe, Coah., México
andres.acosta@cinvestav.edu.mx

A. Humberto Castillejos
professor, Department of Metallurgical Engineering, Centre for Research and Advanced Studies, CINVESTAV – Unidad Saltillo, Ramos Arizpe, Coah., México
humberto.castillejos@cinvestav.edu.mx

Brian G. Thomas
professor, Department of Mechanical Science and Engineering, University of Illinois at Urbana-Champaign, Urbana, Ill., USA
bgthomas@uiuc.edu

Figure 1
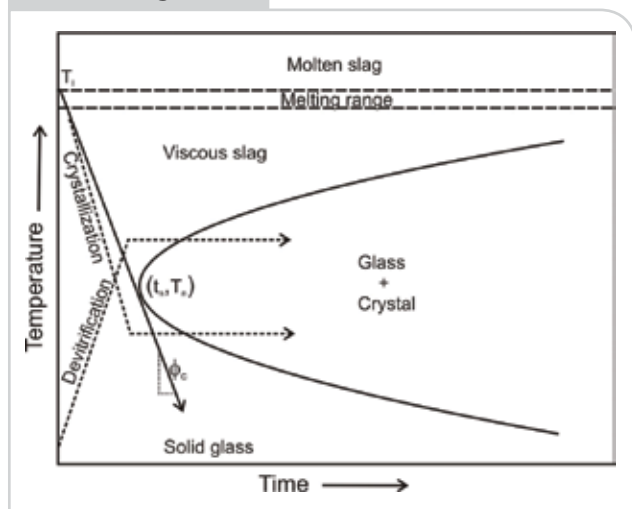
Schematic of a typical nose-shaped TTT diagram showing the melting range, the temperature and time corresponding to the nose tip, the critical cooling rate, a cooling trajectory for crystallization and a heating trajectory for devitrification.

temperature of the hot face of a copper plate slab mold is estimated to range between 200°C and 450°C in compact strip process (CSP) thin-slab molds[10] and still lower in conventional molds,[11] and the steel shell surface is between the liquidus steel temperature and around 1,000°C and 1,150°C in thin[12] and conventional[2] molds, respectively. It might be expected that the liquid slag infiltrating into the mold-strand interspace should solidify as a glassy layer closer to the mold face, where the cooling rates are $>|\phi_c|$ and as a crystalline layer toward the strand surface, where possibly the cooling rates are $<|\phi_c|$. However, as O'Malley and Neal[13] and several others have observed, the actual layering found in flux films recovered from commercial operations is the opposite: the crystalline layer appears on the mold side. The glassy flux film that forms during initial contact with the mold wall remains there long enough to devitrify, even though its temperature is low, so that diffusion is slow. The glass persists near the strand, where temperature is high, perhaps because the undercooling driving force is low. Trajectories for classical crystallization and devitrification are illustrated in Figure 1; the starting points for the trajectories are temperatures equal to or above the liquidus temperature of the slag and temperatures below the glass transition temperature, respectively.

Since the TTT diagrams for glass-forming materials quantify how the phase transformations evolve with temperature history, they are useful tools for designing and selecting mold fluxes. Time-Temperature-Transformation curves have been studied by several researchers using different thechniques.[14–16] In general, these techniques consist of melting and holding a slag sample at an elevated temperature above its melting point before interrupted quenching to the test temperature, where it is held for a specified holding time. The sample is then quenched and inspected for crystalline phases. Repeating this procedure for different isothermal temperatures and holding times generates temperature vs. time data to map formation of the first crystals as a TTT curve for the onset of crystallization. Rocabois, et al.[14] used a resistance furnace to melt and homogenize oxide mixtures in small, sealed crucibles before transferring them to a cooler zone of the furnace for isothermal holding. The cooling rate to reach the isothermal temperature was about 20°C/second. After the holding period, the sealed crucibles were water quenched; the operation from the end of isothermal treatment to quenching took approximately 5–10 seconds. The sample was then cut and the presence of crystals was detected by optical or electronic microscopy. To obtain higher cooling rates, in excess of 150°C/second, and observe the emerging crystals in-situ, single and double hot thermocouple techniques have been developed.[15,16] Even higher cooling rates, up to 1,000°C/second, are possible using an impulse atomization process.[17] These techniques enable information on crystallization under both isothermal and non-isothermal conditions.

The construction of TTT curves from isothermal cooling experiments is a very laborious task. A convenient alternative is differential thermal analysis (DTA). However, this method is limited to slow cooling rates, no more than ~1°C/second.[16] A more fundamental problem for using DTA to study the crystallization behavior is that certain melts, particularly those rich in silica, exhibit crystallization peaks that are difficult to discern, due to slow crystallization kinetics or small heats of crystallization.[18] However, the crystallization peaks under devitrification are normally very clearly detectable and have been useful to study the sequential formation of crystalline species from solid glass slags,[18,19] and to estimate the glass fraction present in solid slag films.[20] Property measurements and characterization of mold powder slags as done by Meng, et al.[17] become very critical for their design and selection in demanding processes, such as high-speed, thin-slab casting.[21–23]

From the previous review, it can be seen that devitrification plays an essential role in the formation of crystalline phases in the solid slag layer located between the strand and the mold. This work presents a novel procedure to calculate TTT curves, which is based on the integration of a Kissinger-type rate equation under isothermal conditions and on the determination of the rate parameters using differential thermal analysis (DTA). The estimated TTT curves agree

Table 1

Basicity and Composition of Mold Powders A and B

Powder	%CaO/ %SiO$_2$	%SiO$_2$	%CaO	%MgO	%Al$_2$O$_3$	%(Na$_2$O+K$_2$O)	%Fe$_2$O$_3$	%MnO	%C$_{free}$	%F
A	1.03–1.15	28–30	31–33	2–3.5	5–6.5	8.5–10	< 1.5	2–3.5	2–3.5	7–9
B	0.89–1.01	32–34	30–32	2.5–3.5	2–3	11–12.5	< 1.5	< 0.1	3–4	6–7

very well with metallographically determined transformations of glass samples treated isothermally. The kinetic model plus the kinetic information obtained by DTA constitute a powerful combination that simplifies the generation of TTT diagrams.

Experimental Technique

Materials — Two commercial mold powders, denoted as A and B, in bags of 25 kg were decarburized in batches of 100 g in porcelain lab dishes. Six dishes at a time were introduced in a muffle at 650°C for 16 hours, removing the dishes after 5 and 10 hours to mix their charges to ensure complete decarburization. The decarburized powder was ground in an alumina balls mill to a mesh of –100 (–149 µm). The entire amounts of powders A and B were sealed in buckets with desiccant material. The nominal composition of these mold powders is given in Table 1.

A batch of 19 g of ground mold powder was melted and superheated to 1,300°C in a graphite crucible heated by induction. After maintaining for 5 minutes the molten slag was poured into a brass mold at ~100°C; this temperature was chosen to ensure that the material solidified fully glassy and without experiencing thermal shock. Each rod was cut into disks of ~3.1 mm thickness x ~13.8 mm diameter. Rods exhibiting any crystallization on the surface were

discarded. Figure 2a shows the brass mold together with a poured glass rod and examples of a fully glassy and a crystallized disk.

Differential Thermal Analysis Method — A DTA/TGA apparatus (Pyris Diamond, Perkin-Elmer Inc., Waltham, Mass., USA) was used to obtain the devitrification peaks of glass samples heated from room temperature to ~1,090°C at different heating rates. The molten samples were held for 20 minutes at that temperature and then cooled at different rates to obtain the crystallization peaks. The upper temperature and holding time were selected to minimize weight loss of the samples. The heating and cooling rates employed in the consecutive devitrification and crystallization tests are given in the plots showing the DTA curves (Figure 4). When the programmed cooling rate did not match the actual rate, a time average around the crystallization peak(s) is reported. For all the tests, the glass powder employed was obtained by grinding glass disks to sizes between –230 and +270 meshes (i.e., between –63 and +53 µm). The experiments were conducted in Pt containers in a static air atmosphere and using high-purity (99.999%) Al$_2$O$_3$ as a reference material supplied by Perkin-Elmer. The apparatus was periodically calibrated using In, Zn, Au and CuSO$_4$·5H$_2$O standards. The weight of the glass samples loaded to the containers was between 14.95 and 15.05 mg.

Figure 2

(a)   **(b)**
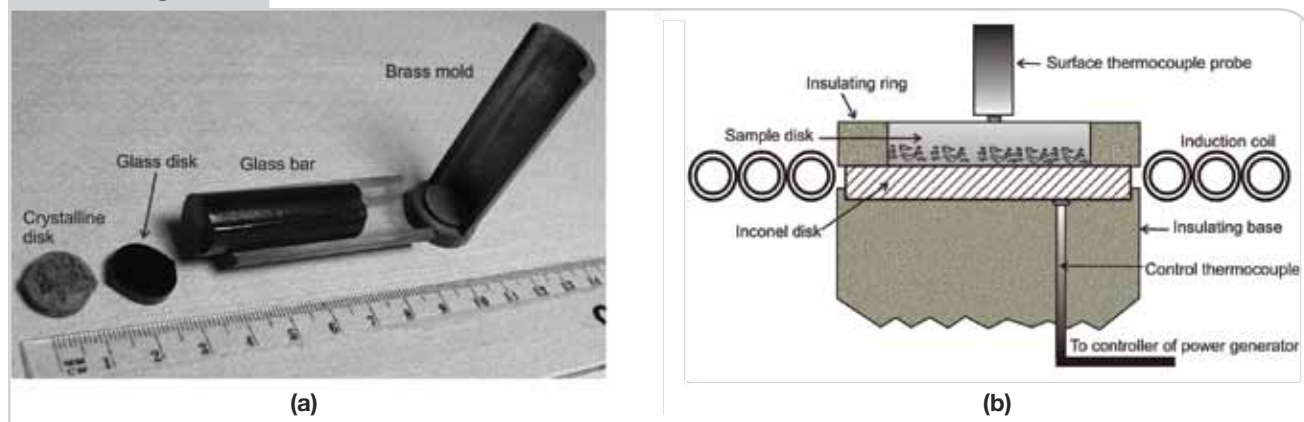
Brass mold for casting glass bars (a) and heating arrangement for isothermal treatment tests (b).

Figure 3

(a)

(b)
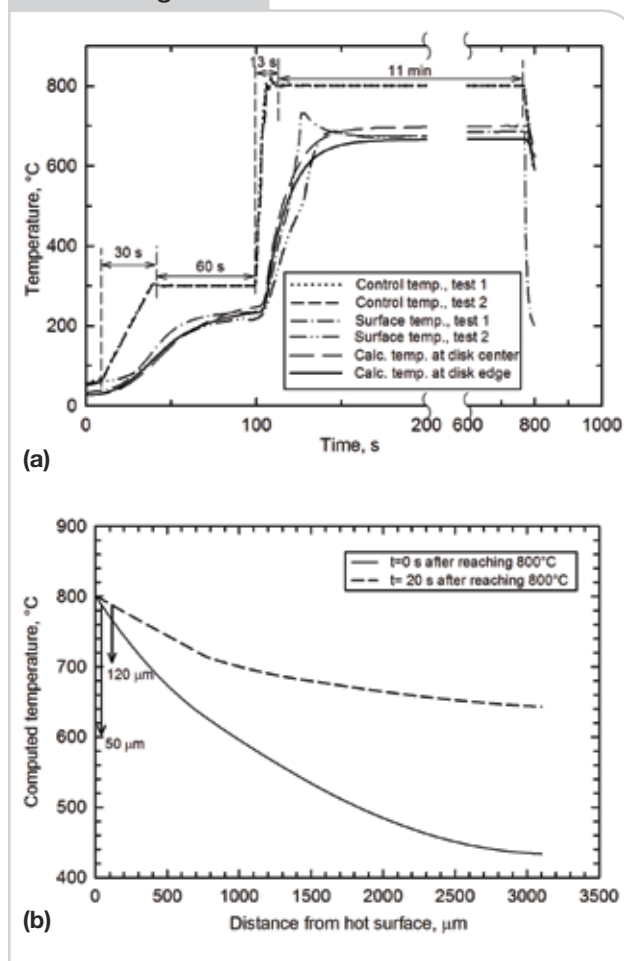
Temperature history of hot plate (control temperature), upper surface of disk (surface temperature) and model predictions (a); and variation of temperature with thickness position at the start of the isothermal plateau and 20 seconds later (b). An 800°C treatment plateau lasting 11 minutes is presented.

Isothermal Treatments — To heat treat the glass disks under isothermal conditions, an Inconel 601 circular plate was inductively heated using a 5 kW high-frequency (HF) generator (Luzars URF-5, ASEPSA S.A. de C.V., QRO, Mexico) with a three-turn flat induction coil. The heating arrangement is shown in Figure 2b. The heating plate was placed in the center of the coil and was instrumented with a K-type thermocouple connected to a controller interfaced to the HF generator. The controller was programmed to make the plate follow prescribed thermal trajectories, such as those presented in Figure 3a. The plate was heated from room temperature to 300°C in 30 seconds and held for 60 seconds. This temperature plateau was required to avoid thermal shock of the sample, and it did not cause any crystallization of the glass disk. The plate was then heated to the final

isothermal treatment temperature in 13 seconds independently of the isothermal temperature prescribed. The temperatures and times of the treatment plateaus are given in the section on Validation of the Predicted TTT Curves.

Before starting each heat treatment experiment, the Inconel plate was polished with emery papers 800 and 1200 and the transverse surfaces of the glass disks were polished up to colloidal silica suspension of 0.05 μm. To initiate an experiment, a glass disk fitted with a thermally insulating ceramic ring was placed on the hot plate. With the disk in place, a contact thermocouple was seated on its upper surface. Measurement of this surface temperature allowed estimation of the thermal evolution of the disk for calculating the thickness of the region approaching isothermal conditions. This region was predicted to be no more than 10°C below the isothermal treatment temperature when the hot plate reached it. Figure 3b shows predicted temperature profiles through the thickness of the disk at two times during the isothermal treatment stage. These calculations are important to accurately define where the metallographic analysis should be done, in order to follow the progress of crystallization under nearly isothermal conditions. The heat conduction model developed for doing the predictions is described elsewhere.[24] After the isothermal treatment, the sample was removed rapidly (two to three seconds) from the heating plate and put to cool on top of a quartz plate at room temperature, without the ceramic ring and while air was blown gently.

For metallographic observation, the treated disks were mounted in an epoxy resin; afterward, they were cut through the longitudinal middle plane to be able to observe both the longitudinal and the transverse (i.e., surface seated on the hot plate) surfaces. The transverse surface was minimally roughed down to avoid removing material that had been in contact with the hot plate. On the other hand, the longitudinal surface was polished to colloidal silica suspension of 0.05 μm and etched for three seconds with a Nital 2% solution. The samples were observed in stereoscopic and scanning electron microscopes (SEM). The zones analyzed by SEM were within 50–120 μm of the hot face, ensuring that isothermal conditions were met.

Results and Discussion

DTA Results and Kinetic Parameters for Devitrification and Crystallization Reactions — DTA curves for mold powders A and B are shown in Figures 4a and 4b, respectively, for various heating rates. Devitrification trajectories from 400°C to ~1,090°C and crystallization trajectories in the opposite direction are shown;

to distinguish between both paths, lines of the same type but different thicknesses are employed in the figures. As seen in Figure 4a, powder A exhibited only one exothermic peak in the temperature ranges covered during devitrification and crystallization, and powder B presented two peaks that are very well defined along devitrification, but the second peak appeared only subtly at a cooling rate of –30°C/minute during crystallization, as observed in Figure 4b. During devitrification, the second peak was already small, and in the course of crystallization did not always show up for the reasons[17] indicated earlier. For powder A, the peak corresponded to the formation of cuspidine, and for mold powder B, the higher peak corresponded also to this mineral and the shorter one to combeite.[24] In the case of powder A, a magnification of the traces corresponding only to the temperature range of the crystallization peak is shown as an inset. Since different crystallization conditions such as heating rate, particle size[25] and nucleation temperatures will cause variations in the DTA curves, as mentioned earlier, the glass used for each of the powders

was treated similarly and had the same granulometry (between 53 and 63 µm). Therefore, the shift exhibited by the DTA curves was associated with the different heating rates used in the experiments. In devitrification, the exothermic peak shifted to higher temperatures and became taller with increasing heating rate, while in crystallization, the peak shifted to lower temperatures but also became higher with increasing cooling rate. As was indicated in the classical studies of Kissinger,[26,27] this variation of the peak with the heating rate, if all other experimental conditions are maintained constant, indicates that the reaction rate varies with temperature, i.e., the reaction requires an activation energy to proceed.

The Kissinger equation,[27] which relates the kinetic parameters for a transformation reaction, is given as:

$$\ln\frac{|\phi|}{T_m^2} = \left(\ln(A\,n\,(1-x_m)^{n-1}) - \ln\frac{|E|}{R} \right) - \frac{E}{R}\left(\frac{1}{T_m} \right)$$

(Eq. 1)

Figure 4
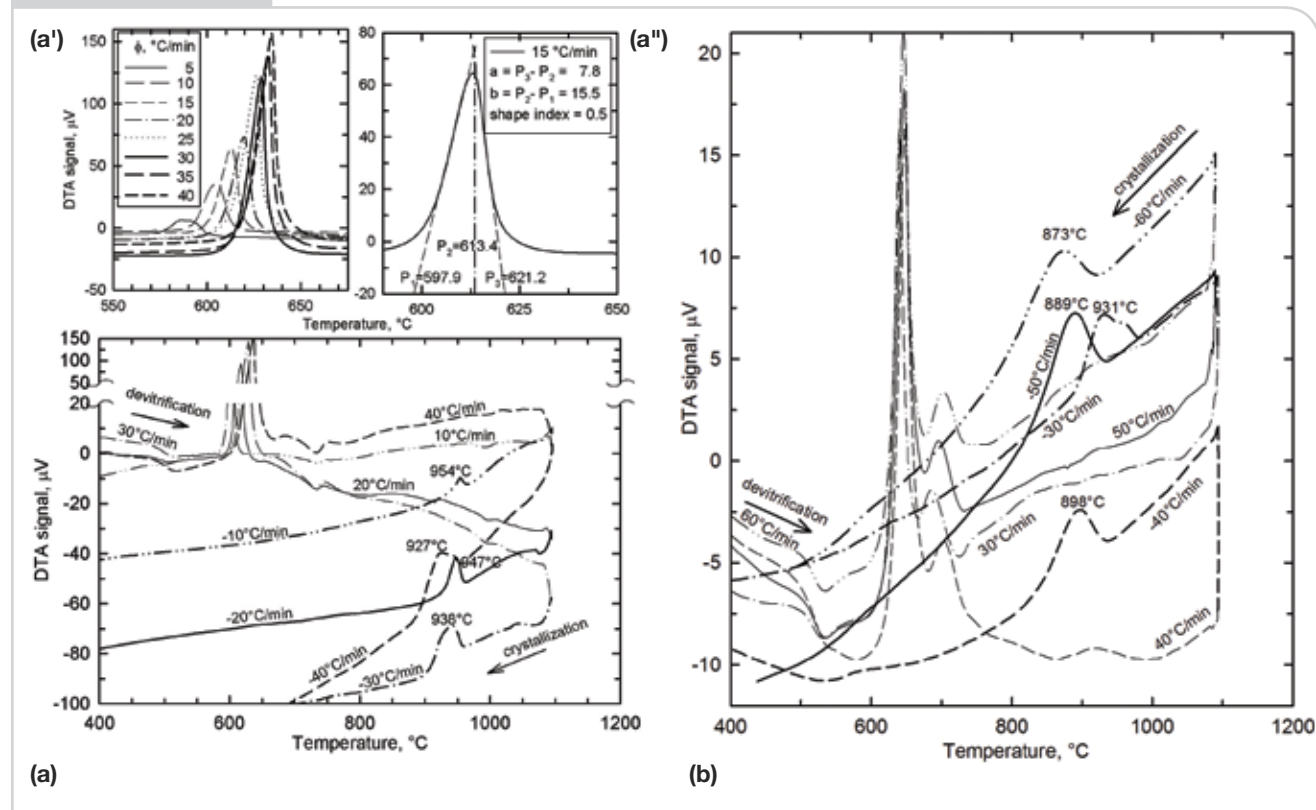
DTA heating and cooling curves at different heating and cooling rates for: mold powder A (with insets (a') and (a")); (a) and mold powder B (b). Some T_m temperatures are indicated close to the peaks.

where

T_m and x_m are the temperature and the fraction of material reacted at the peak,
ϕ is the heating or cooling rate,
n, A and E are the empirical order of reaction, frequency factor and activation energy for crystals formation, respectively, and
R is the gas constant.

The crystalline fraction formed when the maximum of the transformation rate is reached was obtained by graphical integration of the area below the DTA curve up to T_m. The T_m values arising to different cooling rates are displayed in Figures 4a and 4b. Since the transformation peaks for both powders are basically symmetric, as observed in the inset (a') of Figure 4a, the fraction x_m was determined to be very close to an average value of 0.5. The order of reaction n was evaluated from the relation obtained by Kissinger, indicating that:

$$n = 1.26\, S^{1/2}$$

(Eq. 2)

where

S is the shape index defined as the absolute ratio of the slopes of tangents to the transformation curve at the inflexion points, as illustrated in inset (a") of Figure 4a.

According to Kissinger Equation 1, a plot of $\ln\left(\phi / T_m^2\right)$ vs. T_m should be a line with a slope $-E/R$ and with an abscissa from which A can be evaluated. The Kissinger lines corresponding to the devitrification of glass samples of powders A and B are displayed in Figure 5, and the legend box includes the values of the kinetic parameters. Thus, it is seen that the formation of crystals during devitrification follows the Kissinger model and that, although the energies of activation are quite similar, the positions of the lines for the two powders are noticeably different due to the values of A and n; additionally, the reproducibility among experiments is quite good. The lines in Figure 5 appear to demonstrate that, under well-controlled DTA conditions and sample preparation, the position of the lines for the devitrification taking place during the heating of mold powder glasses is controlled by the transformation reaction or reactions resulting from the mold powder

nature. The lines obtained for the crystallization occurring during cooling of the mold powder slags are presented elsewhere.[24]

New Method for Determining the Rate of Isothermal Transformation for Generating TTT Diagrams — As seen in the previous section, the Kissinger method allows obtaining kinetic parameters of phase transformations occurring during non-isothermal conditions. However, to the best of the authors' knowledge, this information has not been used to predict the progress of isothermal transformations as a function of time. Assuming that the equation used by Kissinger, to describe the kinetics of decomposition reactions of carbonates and hydroxides, is valid also for the crystallization of amorphous materials, then the rate of transformation of a glassy material can be given as:
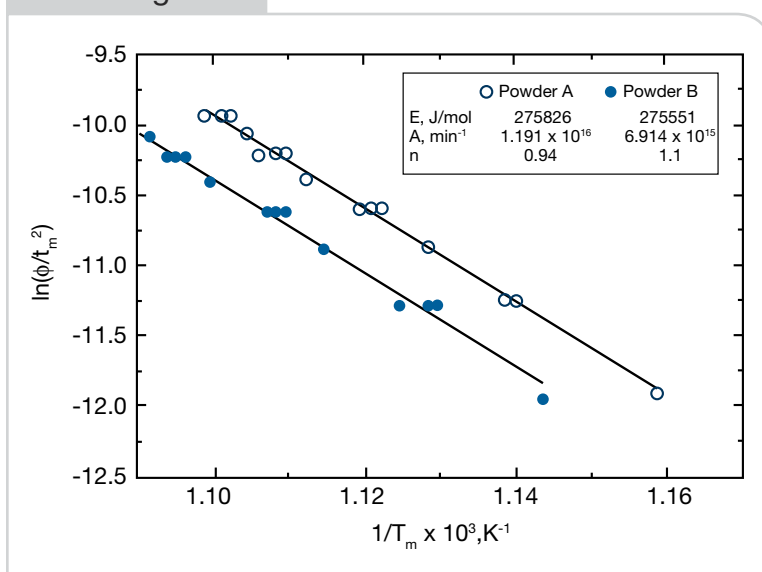
$$\frac{dx}{dt} = A(1-x)^n\, e^{-\frac{E}{RT}} = k(1-x)^n$$

Eq. (3)

where

k is a rate constant that depends on temperature and, as seen experimentally in the previous section, n A and E are independent of it.

Integrating Equation 3 from $t = 0$ to $t = t$ and $x = 0$ to $x = x$, at constant T, then the time t required to obtain a given transformation fraction x can be written as:

Figure 5

Kissinger lines for the devitrification of mold powders A and B. The values of the kinetic parameters are shown in the legend.

$$t = \left(\frac{1 - (1 - x)^{1-n}}{k} \right) \left(\frac{1}{1-n} \right)$$

(Eq. 4)

Thus, considering that the onset and conclusion of crystallization are given by the times when x = 0.01 and 0.99, respectively, it is possible to calculate the TTT curves for a transformation characterized by particular kinetic parameters.

Based on the slower cooling rates required for producing the fully glassy rods described in the section entitled "Materials," and on the results of a heat conduction model[24] regarding the cooling rates prevailing during the solidification of glass bars, it was

considered appropriate to introduce in Equation 4 an incubation time τ, such that,

$$t = \tau + \left(\frac{1 - (1 - x)^{1-n}}{k} \right) \left(\frac{1}{1-n} \right)$$

(Eq. 5)

For the powders studied, τ = 10 seconds was specified. The predicted TTT diagrams for powders A and B are represented by the lines plotted in Figures 6 and 7, respectively. The lower parts of the TTT curves were computed from the DTA heating curves, while the upper parts were calculated from the DTA cooling curves; i.e., they were computed from devitrification and crystallization DTA tests, respectively. The onset and conclusion of crystallization are indicated by the TTT curves.

The predicted TTT diagrams for both powders are quite similar at temperatures below 600°C, but above 700°C they exhibit differences, particularly in regard to the conclusion of crystallization. According to the diagrams, powder B requires considerably longer times to accomplish crystallization at temperatures between 800°C and 900°C. The predicted similarities and differences in the TTT diagrams are validated by the metallographic analysis of isothermally treated disks presented in the following section.

Validation of the Predicted TTT Curves — The letters plotted in Figures 6 and 7 indicate the temperatures and times of the isothermal plateaus at which a thin region of the glass disks was subjected while seated on the hot plate; lowercase letters designate the treatments of mold powder A, and uppercase letters those for mold powder B. Corresponding low-magnification stereoscopic images of the entire longitudinal cross-section of treated disks, together with photomicrographs taken within the isothermal region, are displayed in Figures 8 and 9. Agreeing with the TTT diagrams, the microstructures a, b, c, and d are very similar to those observed in the photomicrographs A, B, C and D. As expected from the TTT diagrams, the photomicrographs a, b, c, A, B and C show almost completely uniform glassy structures except for some bright spots that appear commonly in samples that are just starting to crystallize. These spots are minute regions, rich in iron,
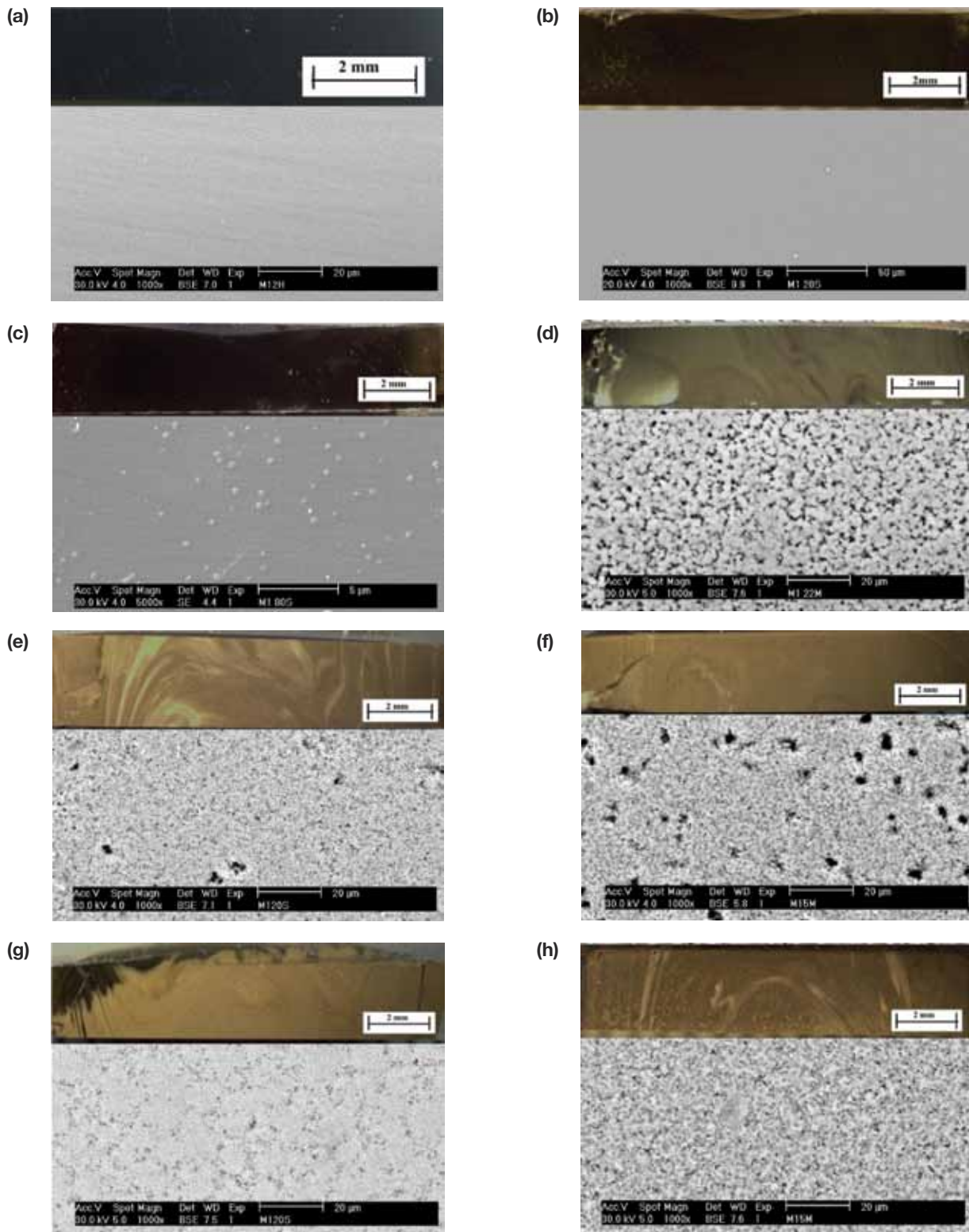
Figure 6
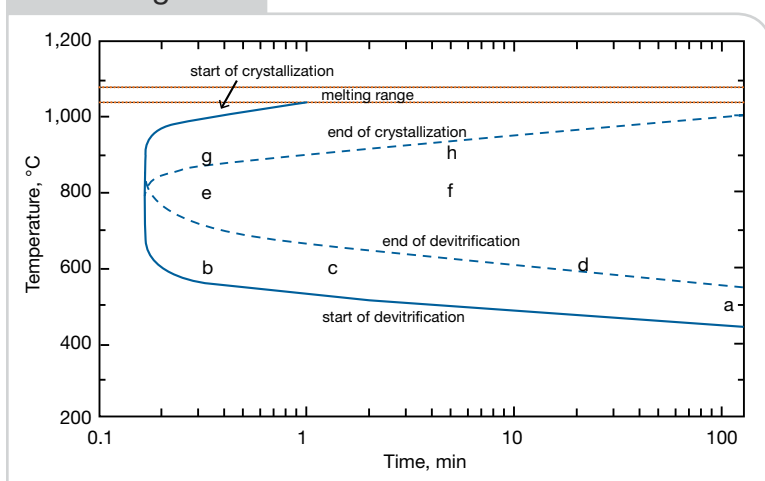
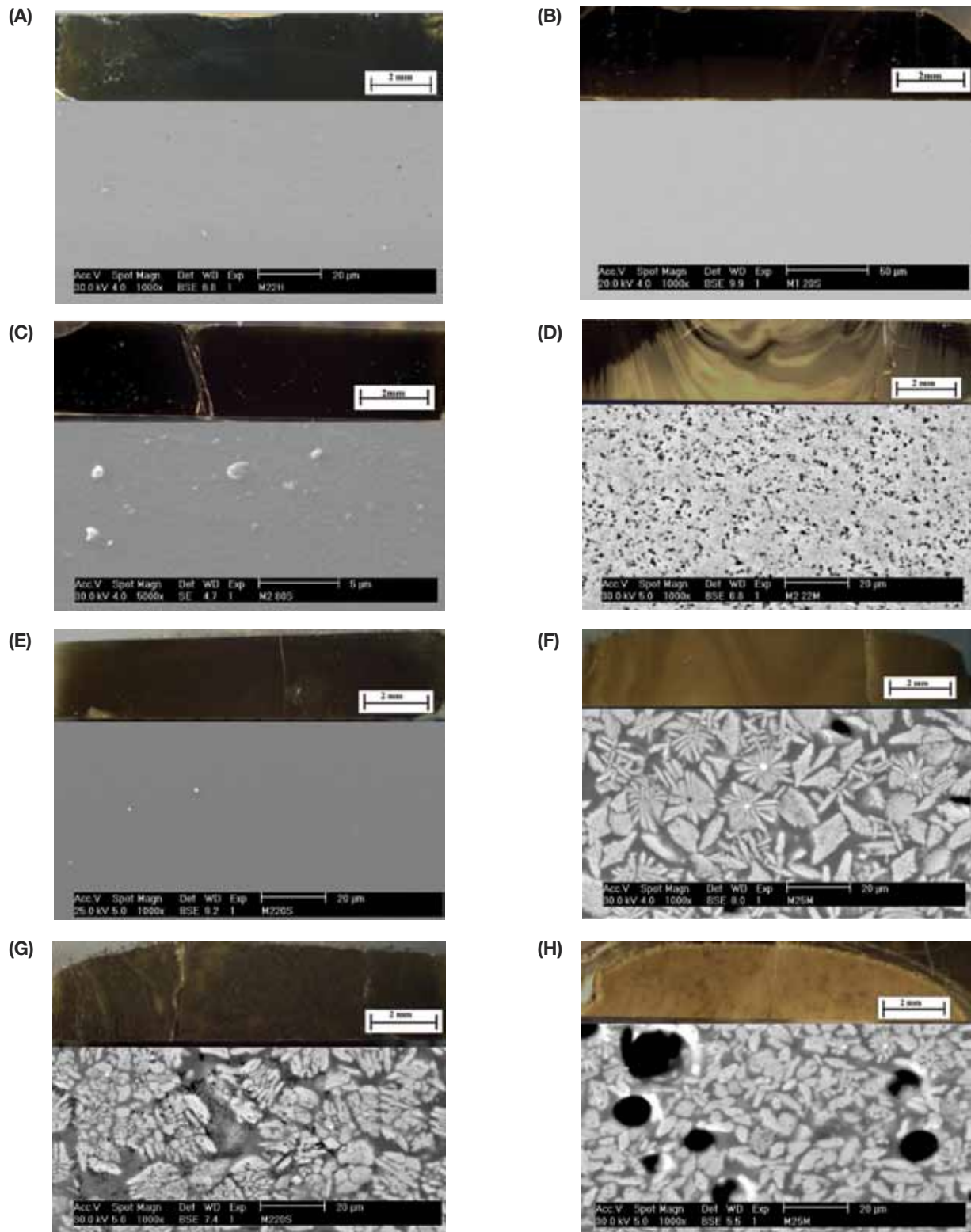TTT diagram for powder A.

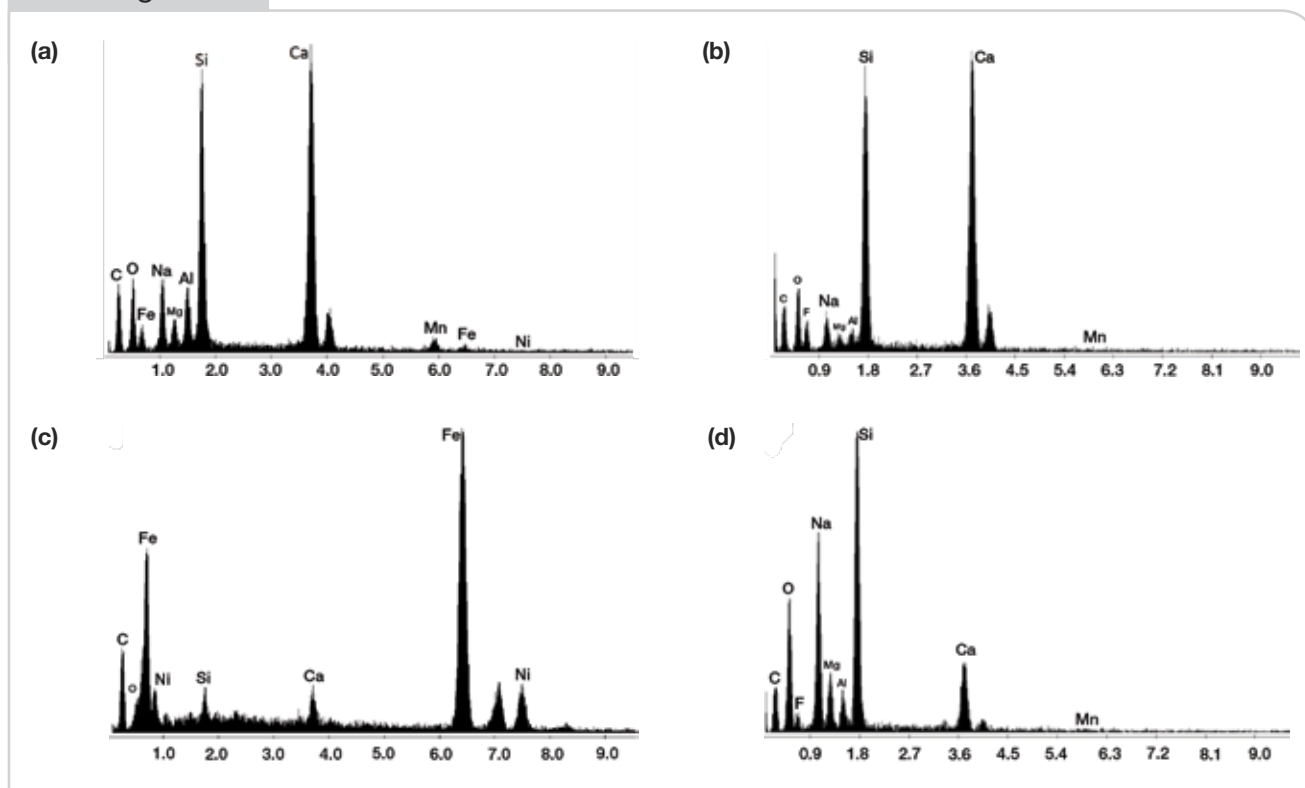## Figure 7
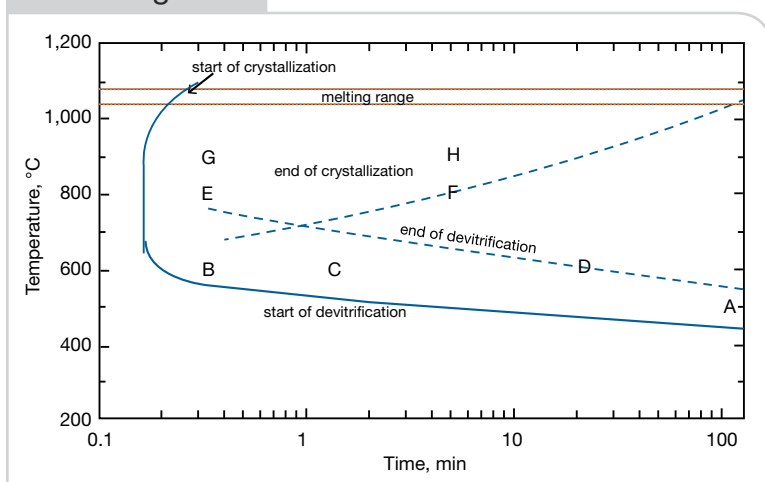
TTT diagram for powder B.

Figure 8

Low-magnification stereoscopic images and SEM photomicrographs of disks of mold powder A, devitrified under different conditions: 500°C, 120 minutes (a); 600°C, 20 seconds (b); 600°C, 80 seconds (c); 600°C, 22 minutes (d); 800°C, 20 seconds (e); 800°C, 5 minutes (f); 900°C, 20 seconds (g); and 900°C, 5 minutes (h). The photomicrographs were obtained in the backscattered electrons (BSE) imaging mode, except for (c), where the secondary electrons (SE) imaging mode was employed.

Low-magnification stereoscopic images and SEM photomicrographs of disks of mold powder B, devitrified under different conditions: 500°C, 120 minutes (A); 600°C, 20 seconds (B); 600°C, 80 seconds (C); 600°C, 22 minutes (D); 800°C, 20 seconds (E); 800°C, 5 minutes (F); 900°C, 20 seconds (G); and 900°C, 5 minutes (H). The photomicrographs were obtained in the backscattered electrons (BSE) imaging mode, except for (C), where the secondary electrons (SE) imaging mode was employed.

Figure 10

Energy dispersive x-ray microanalysis spectra for mold powder A treated at 600°C for 20 seconds (Figure 8(b)): in glass matrix (a); and in small bright spots (b); for mold powder B treated at 800°C for 5 minutes (Figure 9F): in flower-shaped crystals (c); and in glass matrix (d).

that form early in the process and that possibly act as nucleation sites for cuspidine. Energy dispersive x-ray (EDX) microanalysis spectra of the matrix and of a spot in sample b are presented in Figures 10a and 10b, respectively; spots in samples a, c, A, B, and C showed similar spectra. As expected from the TTT diagrams the photomicrographs d and D show very similar and high transformation degrees.

The marked difference in the transformation of powders A and B predicted by the TTT diagrams at 800°C for conditions e and E are confirmed by the respective microstructures observed in Figures 8e and 9E. Also, in agreement with the TTT diagrams, the microstructures in Figures 8f and 9F show a large degree of crystallization in both cases, but since this process occurred much faster in mold powder A than B, the crystals obtained are much smaller in the first than in the second powder. A behavior similar to this is observed under conditions g, h, G and H, but as expected from the TTT diagrams, with a smaller degree of crystallization in the case of powder B. For this powder, EDX microanalysis spectra of the crystalline and glassy zones are shown in Figures 10c and 10d; the glass zone is rich in Na and poor in Ca.

The TTT diagrams and the isothermal treatments reveal that powders A and B differentiate themselves by their distinct tendency to crystallize at temperatures higher that 800°C, but below that temperature their behaviors for crystallization are similar. It should be noted that all the isothermal treatment results were obtained under devitrification conditions, and that for temperatures above T_n they were compared with TTT curves generated from DTA cooling curves for crystallization. The agreement of both kinds of results suggests that heating a solid sample to a sufficiently high temperature leads to the same crystallization outcome as cooling of a liquid sample to that temperature. The stereoscopic images included in Figures 8 and 9 show the different opacity of glass disks treated isothermally at different T and t. However, low magnifications are not sufficient to judge the tendency of a powder to crystallize.

Summary and Conclusions

A novel procedure to calculate TTT curves of mold slags is demonstrated in this work. This is based on the integration under isothermal conditions of a Kissinger-type rate equation using rate parameters determined from differential thermal analysis (DTA). The estimated TTT curves agree very well

with transformations observed metallographically by inspecting thin glass disks treated isothermally and quenched.

Acknowledgments

References

1. J.K. Brimacombe and K. Sorimachi, "Crack Formation in the Continuous Casting of Steel," *Metallurgical and Materials Transactions B,* Vol. 8B, 1977, pp. 489–505.

2. A. Grill, K. Sorimachi and J.K. Brimacombe, "Heat Flow, Gap Formation and Breakouts in the Continuous Casting of Steel Slabs," *Metallurgical and Materials Transactions,* Vol. 7B, 1976, pp. 177–189.

3. Y. Meng and B.G. Thomas, "Simulation of Microstructure and Behavior of Interfacial Mold Slag Layer in Continuous Casting of Steel," *ISIJ International,* Vol. 46, 2006, pp. 660–669.

4. R. Bommaraju, "Optimum Selection and Application of Mold Fluxes for Carbon Steels," *74th Steelmaking Conference Proceedings,* Washington, D.C., Vol. 74, 1991, pp. 131–146.

5. H. Kyoden, T. Doihara and O. Nomura, "Development of Mold Powders for High-Speed Continuous Casting of Steel," *69th Steelmaking Conference Proceedings,* Washington, D.C., Vol. 69, 1986, pp.153–159.

6. J.W. Cho and H. Shibata, "Effect of Solidification of Mold Fluxes on the Heat Transfer in Casting Mold," *Journal of Non-Crystalline Solids,* Vol. 281, 2001, pp. 110–117.

7. K. Watanabe, M. Suzuky, K. Murakami, H. Kondo and T. Shiomi, "Development of Mold Powder for High-Speed Casting of Middle Carbon Steel," *79th Steelmaking Conference Proceedings,* Pittsburgh, Pa., Vol. 79, 1996, pp. 265–268.

8. D. Jiang, X. Bing, X. Jianping and J. Chengqing, "Radiative Heat Transfer in Transition Metal Oxides Contained in Mold Fluxes," *ISIJ International,* Vol. 49, 2009, pp. 1710–1714.

9. S. Feldbauer, I. Jimbo, A. Sharan, K. Shimuzu, W. King, J. Stepanek, J. Harman and A.W. Cramb, "Physical Properties of Mold Slags That Are Relevant to Clean Steel Manufacture," *78th Steelmaking Conference Proceedings,* Nashville, Tenn., Vol. 78, 1995, pp. 655–668.

10. J.E. Camporredondo S., A.H. Castillejos E., F.A. Acosta G., E.P. Gutierrez M. and M.A. Herrera G., "Analysis of Thin-Slab Casting by the Compact Strip Process: Part I. Heat Extraction and Solidification," *Metallurgical and Materials Transactions,* Vol. 35B, 2004, pp. 541–560.

11. I.V. Samarasekera and J.K. Brimacombe, "The Thermal Field in Continuous Casting Molds," *Canadian Metallurgical Quarterly,* Vol. 18, 1979, pp. 251–266.

12. J.J. Montes R., A. Castillejos E., F.A. Acosta G., E.P. Gutiérrez M. and M.A. Herrera G., "Effect of the Operating Conditions of Air Mist Nozzles on the Thermal Evolution of Continuously Cast Thins Slabs," *Canadian Metallurgical Quarterly,* Vol. 47, 2008, pp. 187–204.

13. R.J. O'Malley and J. Neal, "An Examination of Mold Flux Film Structures and Mold Gap Behavior Using Mold Thermal Monitoring and Petrographic Analysis at Armco's Mansfield Operations," *METEC Congress 99,* Düsseldorf, Vol. 1, 1999, pp. 188–195.

14. P. Rocabois, J.N. Pontoire, J. Lehmann and H. Gaye, "Crystallization Kinetics of Al_2O_3-CaO-SiO_2-Based Oxide Inclusions," *Journal of Non-Crystalline Solids,* Vol. 282, 2001, pp. 98–109.

15. Y. Kashiwaya, C.E. Cicutti, A.W. Cramb and K. Ishii, "Development of Double and Single Hot Thermocouple Technique for In-Situ Observation and Measurement of Mold Slag Crystallization," *ISIJ International,* Vol. 38, 1998, pp. 348–356.

16. W. Guang-hua, I. Hui and T. Ping, "CCT and TTT Diagrams to Characterize Crystallization Behavior of Mold Fluxes," *Journal of Iron and Steel Research,* Vol. 15, 2008, pp. 32–37.

17. Y. Meng, B.G. Thomas, A.A. Polycarpou, A. Prasad and H. Henein, "Mold Slag Property Measurements to Characterize CC Mold — Shell Gap Phenomena," *Canadian Metallurgical Quarterly,* Vol. 45, 2006, pp. 79–94.

18. C.S. Ray, S.T. Reis, R.K. Brow, W. Höland and V. Rheinberger, "A New DTA Method for Measuring Critical Cooling Rate for Glass Formation," *Journal of Non-Crystalline Solids,* Vol. 351, 2005, pp. 1350–1358.

19. M. Dipiaggi, G. Artroli, C. Righi and R. Carli, "High-Temperature Reactions in Molten Flux Slags: Kinetic Versus Composition Control," *Journal of Non-Crystalline Solids,* Vol. 353, 2007, pp. 2852–2860.

20. K.C. Mills, L. Courtney, A.B. Fox, B. Harris, Z. Idoyaga and M.J. Richardson, "The Use of Thermal Analysis in the Determination of the Crystalline Fraction of Slags Films," *Termochimica Acta,* Vol. 391, 2002, pp. 175–184.

21. F. Neumann, J. Neal, M.A. Pedroza, A.H. Castillejos E. and F.A. Acosta G., "Mold Fluxes for High-Speed Slab Casting," *79th Steelmaking Conference Proceedings,* Pittsburgh, Pa., Vol. 79, 1996, pp. 249–257.

22. D. Blevins, M. Ingold, A. Schaefer, J. Neal, F. Neumann and C. Sowa, "Mold Powder Performance: Steel Dynamics' High-Speed Thin-Slab Casters," *Ironmaking Steelmaking,* Vol. 27, 2000, pp. 85–88.

23. J.A. Kromhout, S. Melzer, E.W. Zinngrebe, A.A. Kamperman and R. Boom, "Mold Powder Requirements for High-Speed Casting," *Steel Research International,* Vol. 79, 2008, pp. 143–148.

24. Y.G. Maldonado, third Ph.D. progress report, CINVESTAV – Unidad Saltillo, Coah., México, 2011.

25. W. Li and B.S. Mitchell, "Nucleation and Crystallization in Calcium Aluminate Glasses," *Journal of Non-Crystalline Solids,* Vol. 255, 1999, pp. 199–207.

26. H.E. Kissinger, "Variation of Peak Temperature With Heating Rate in Differential Thermal Analysis," *Journal of Research of the National Bureau of Standards,* Vol. 57, 1956, pp. 217–221.

27. H.E. Kissinger, "Reactions Kinetics in Differential Thermal Analysis," *Analytical Chemistry,* Vol. 29, 1957, pp. 1702–1706.

✦

Nominate this paper